Athermal silicon nitride angled MMI wavelength division (de)multiplexers for the near-infrared

Thalía Domínguez Bucio,[1,*] Ali Z. Khokhar,[1] Goran Z. Mashanovich,[1] and Frederic Y. Gardes[1]

[1] *Optoelectronics Research Centre, University of Southampton, Southampton SO17 1BJ, UK*
[*] *tdb2g12@soton.ac.uk*

Abstract:
WDM components fabricated on the silicon-on-insulator platform have transmission characteristics that are sensitive to dimensional errors and temperature variations due to the high refractive index and thermo-optic coefficient of Si, respectively. We propose the use of NH_3-free SiN_x layers to fabricate athermal (de)multiplexers based on angled multimode interferometers (AMMI) in order to achieve good spectral responses with high tolerance to dimensional errors. With this approach we have shown that stoichiometric and N-rich SiN_x layers can be used to fabricate AMMIs with cross-talk<30dB, insertion loss <2.5dB, sensitivity to dimensional errors <120pm/nm, and wavelength shift <10pm/°C.

OCIS codes: (130.0130) Integrated optics; (130.3120) Integrated optics devices; (130.7408) Wavelength filtering devices.

References and links

1. L. Wang, W. Bogaerts, P. Dumon, S. K. Selvaraja, J. Teng, S. Pathak, X. Han, J. Wang, X. Jian, M. Zhao, R. Baets, and G. Morthier, "Athermal arrayed waveguide gratings in silicon-on-insulator by overlaying a polymer cladding on narrowed arrayed waveguides," Appl. Opt. **51**, 1251–1256 (2012).
2. W. Bogaerts, S. K. Selvaraja, P. Dumon, J. Brouckaert, K. D. Vos, D. V. Thourhout, and R. Baets, "Silicon-on-Insulator Spectral Filters Fabricated With CMOS Technology," IEEE J. Sel. Top. Quantum Electron. **16**, 33–44 (2010).
3. J. M. Lee, D. J. Kim, H. Ahn, S. H. Park, and G. Kim, "Temperature Dependence of Silicon Nanophotonic Ring Resonator With a Polymeric Overlayer," J. Light. Technol. **25**, 2236–2243 (2007).
4. Y. Hu, R. M. Jenkins, F. Y. Gardes, E. D. Finlayson, G. Z. Mashanovich, and G. T. Reed, "Wavelength division (de) multiplexing based on dispersive self-imaging," Opt. Lett. **36**, 4488–4490 (2011).
5. Y. Hu, F. Y. Gardes, D. J. Thomson, G. Z. Mashanovich, and G. T. Reed, "Coarse wavelength division (de)multiplexer using an interleaved angled multimode interferometer structure," Appl. Phys. Lett. **102**, 7–11 (2013).
6. Y. Hu, T. Li, D. J. Thomson, X. Chen, J. S. Penades, a. Z. Khokhar, C. J. Mitchell, G. T. Reed, and G. Z. Mashanovich, "Mid-infrared wavelength division (de)multiplexer using an interleaved angled multimode interferometer on the silicon-on-insulator platform." Opt. Lett. **39**, 1406–9 (2014).
7. Y. Hu, D. J. Thomson, F. Y. Gardes, G. Z. Mashanovich, and G. T. Reed, "The evolution of angled MMI structure on the SOI platform," Proc. SPIE **8990**, 89900E–89900E–6 (2014).
8. M. Uenuma and T. Motooka, "Temperature-independent silicon waveguide optical filter," Opt. Lett. **34**, 599–601 (2009).
9. T. Domínguez Bucio, A. Z. Khokhar, C. Lacava, S. Stankovic, G. Z. Mashanovich, P. Petropoulos, and F. Y. Gardes, "Material and optical properties of low-temperature NH 3 -free PECVD SiN x layers for photonic applications," J. Phys. D. Appl. Phys. **50**, 025106 (2017).
10. C. Lacava, S. Stankovic, A. Z. Khokhar, T. D. Bucio, F. Gardes, G. T. Reed, D. J. Richardson, and P. Petropoulos, "Si-rich Silicon Nitride for Nonlinear Signal Processing Applications," Sci. Rep. pp. 1–13 (2016).
11. K. Debnath, T. Domínguez Bucio, A. Al-Attili, A. Z. Khokhar, S. Saito, and F. Y. Gardes, "Photonic crystal waveguides on silicon rich nitride platform," Opt. Express **25**, 3214–3221 (2017).
12. A. V. Krishnamoorthy, R. Ho, X. Zheng, H. Schwetman, J. Lexau, P. Koka, G. Li, I. Shubin, and J. E. Cunningham, "Computer Systems Based on Silicon Photonic Interconnects," Proc. IEEE **97**, 1337–1361 (2009).
13. S. Selvaraja, W. Bogaerts, P. Dumon, D. Van Thourhout, and R. Baets, "Subnanometer linewidth uniformity in silicon nanophotonic waveguide devices using CMOS fabrication technology," IEEE J. Sel. Top. Quantum Electron. **16**, 316–324 (2010).
14. P. Dong, "Silicon photonic integrated circuits for wavelength-division multiplexing applications," IEEE J. Sel. Top. Quantum Electron. **22** (2016).
15. A. Kaneko, T. Goh, H. Yamada, T. Tanaka, and I. Ogawa, "Design and applications of silica-based planar lightwave circuits," IEEE J. Sel. Top. Quantum Electron. **5**, 1227–1236 (1999).

16. N. Keil, H. Yao, C. Zawadzki, J. Bauer, M. Bauer, C. Dreyer, and J. Schneider, "Athermal all-polymer arrayed-waveguide grating multiplexer," Electron. Lett. **37**, 579 (2001).
17. J. Soole, M. Schlax, C. Narayanan, and R. Pafchek, "Athermalisation of silica arrayed waveguide grating multiplexers," Electron. Lett. **39**, 1182 (2003).
18. N. Rouger, L. Chrostowski, and R. Vafaei, "Temperature effects on silicon-on-insulator (SOI) racetrack resonators: a coupled analytic and 2-D finite difference approach," J. Light. Technol. **28**, 1380–1391 (2010).
19. J. Teng, P. Dumon, W. Bogaerts, H. Zhang, X. Jian, X. Han, M. Zhao, G. Morthier, and R. Baets, "Athermal Silicon-on-insulator ring resonators byoverlaying a polymer cladding on narrowedwaveguides," Opt. Express **17**, 14627–14633 (2009).
20. A. Arbabi and L. L. Goddard, "Measurements of the refractive indices and thermo-optic coefficients of Si3N4 and SiO(x) using microring resonances." Opt. Lett. **38**, 3878–81 (2013).
21. F. Qiu, A. M. Spring, F. Yu, and S. Yokoyama, "Complementary metal-oxide-semiconductor compatible athermal silicon nitride/titanium dioxide hybrid micro-ring resonators," Appl. Phys. Lett. **102** (2013).
22. D. Dai, Z. Wang, J. F. Bauters, M.-C. Tien, M. J. R. Heck, D. J. Blumenthal, and J. E. Bowers, "Low-loss Si3N4 arrayed-waveguide grating (de)multiplexer using nano-core optical waveguides," Opt. Express **19**, 14130–14136 (2011).
23. K. Wörhoff, R. G. Heideman, A. Leinse, and M. Hoekman, "TriPleX: a versatile dielectric photonic platform," Adv. Opt. Technol. **4**, 189–207 (2015).

---

1. Introduction

Wavelength division (de)multiplexing (WDM) devices are important elements required to increase the capacity of data-links and high speed telecommunication photonic systems. The most popular WDM integrated technologies include arrayed waveguide gratings (AWG) [1], planar concave gratings (PCG) [2] and micro-ring resonators (RR) [3]. These components usually require sophisticated design processes and complex fabrication steps to achieve low insertion losses and improved spectral responses. More recently, an alternative technology based on dispersive self-imaging in multimode waveguides has also been used to obtain angled multimode interferometers (AMMI) for WDM in the near infra-red (NIR) and mid infra-red (MIR) [4–6]. These AMMI structures have a distinctive ease of fabrication, high tolerance to dimensional errors and low insertion losses compared to other WDM approaches [7].

The vast majority of WDM components have been fabricated on the mature silicon-on-insulator (SOI) platform. However, their transmission characteristics tend to be strongly sensitive to temperature variations due to the relatively high thermo-optic coefficient of Si ($1.8\text{x}10^{-4}$/°C). In fact, the thermal shift produced in the central wavelength of these devices is of the order of 70-100pm/°C in the NIR region [2, 3, 8]. As a result, they require active temperature control or complex compensation techniques to stabilize the wavelength drift in order to preserve their performance at different temperatures.

To tackle this situation, we propose using a recently demonstrated silicon nitride (SiN_x) platform [9–11] with low propagation losses and potentially lower thermo-optic coefficient to fabricate AMMI (de)multiplexers . With this approach we aim to combine the distinctive advantages of the AMMI structures with the advantages of the SiN_x platform in order to demonstrate athermal (de)multiplexers with low insertion losses and spectral tolerance to dimensional errors with a relatively simple fabrication process (i.e. single lithography and single etching steps).

In this paper, we report the design, fabrication and characterisation of two AMMI triplexers for the O (1260-1360nm) and C (1530-1565) telecommunication bands. We discuss the spectral characteristics of both devices and the effect that the refractive index (n) of three different SiN_x layers have on them. Finally, we detail the effect that both temperature and dimensional variations have on the central wavelength of the devices. To the best of our knowledge, the study in this paper is the first demonstration of SiN_x AMMI (de)multiplexers for WDM in the NIR wavelength regime.

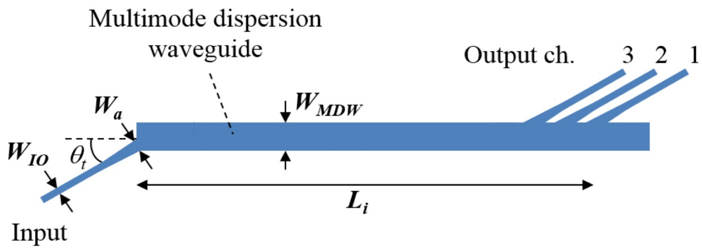

Fig. 1. Schematic of an AMMI.

2. Design and fabrication

Figure 1 shows the basic structure of an AMMI. It consists of a multimode waveguide of width W_{MDW} with input/output waveguides of width W_{IO}. Opposed to conventional multimode interferometers (MMI), the input/output waveguides of the device are tilted at an angle θ_t. Similarly, the input/output waveguides are tapered from its single-mode width to W_a before entering the multimode waveguide to increase the fidelity of the devices. The axial positions of the output waveguides respect to the input (L_i) are designed to match the dispersive self-imaging condition of an MMI given by Equation 1 where, n_{eff} is the effective index of the fundamental mode in the multimode region of the device and λ_i is the design wavelength of the ith output channel [6].

$$L_i = \frac{4 n_{eff} x W_{MDW}^2}{\lambda_i} \qquad (i = 1, 2, 3) \tag{1}$$

The two AMMI triplexers were designed to operate at different wavelength windows within the O band (1270-1320nm) and the C band (1520-1570nm), respectively. Before running simulations, W_{MDW} was fixed at $25\mu m$ so that the dimensions of the designed devices could be comparable to those of previously demonstrated AMMIs on SOI [4, 5]. The rest of the structural parameters were then optimised to provide spectral responses with insertion losses (IL) <2dB and cross-talk (XT) ≈15-20dB using FIMMWAVE with a refractive index of 2.0 for SiN_x.

Figure 2 shows the IL of the devices as a function of W_a using an initial θ_t of 0.3 radians. From these results, W_a was selected to be $9\mu m$ as this value minimises the IL for both wavelength bands. Similarly, θ_t was then adjusted to minimise the XT between adjacent channels. Initial values for (L_i) were calculated to provide a channel spacing ($\Delta\lambda$) ≈15nm using equation 1. Figure 3 depicts the precise (L_i) values obtained for both devices after simulations were performed. Table 1 shows the optimised design parameters for both devices.

Table 1. Optimised design parameters for the 3-channel AMMI

$W_a = 9\mu m, \quad W_{MDW} = 25\mu m$					
λ Band	$\theta_t(rad)$	$W_{io}(nm)$	$L_1(\mu m)$	$L_2(\mu m)$	$L_3(\mu m)$
O (1260-1320nm)	0.29	900	3053	3018	2983
C (1520-1570nm)	0.31	1200	2486	2453	2421

Tapered grating couplers were used to effectively couple light into the devices via optical fibres. Each coupler consists of a single-mode waveguide tapered up to a $10\mu m$ wide waveguide, where surface gratings are incorporated. The period of the gratings was selected to be either

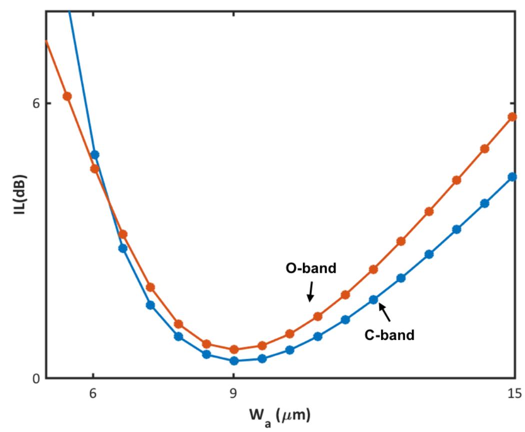

Fig. 2. IL as a function W_a for the C and O bands when $W_{MDW} = 25\mu m$ and $\theta_t = 0.3rad$.

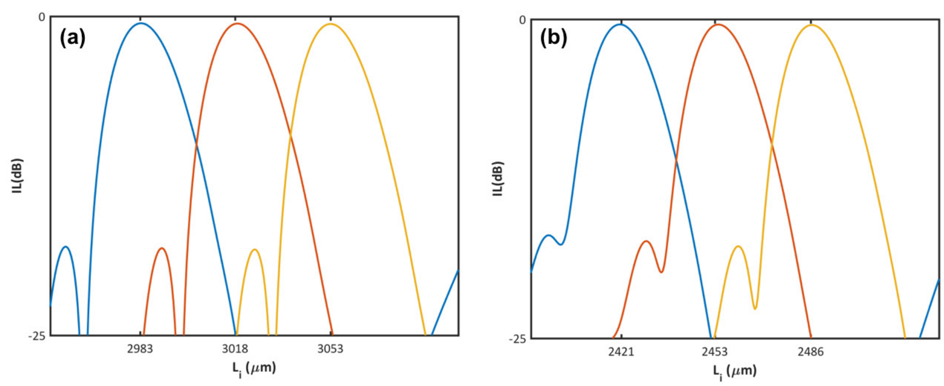

Fig. 3. Optimised L_i for the: (a) O-band and (b) C-band when $W_{MDW} = 25\mu m$ with optimised θ_t.

900 or 1200nm in order to couple the central wavelength of each of the bands studied, O and C respectively.

Several structures were included in the final mask layout to optimize and measure the designed devices. A set of AMMIs with different lengths was considered to account for fabrication errors and to calibrate the output lengths for the desired wavelengths. In addition, AMMI structures with W_{MDW} with variations of ±20 and ±40nm were added to study the sensitivity of the devices to dimensional variations. Finally, a separate structure with two tapered grating couplers connected back-to-back was included for normalization purposes.

The structures were fabricated on three different SiN_x layers with a thickness of 300nm. These layers were deposited on 6" Si wafers with a $2\mu m$ thermally-grown SiO_2 layer using the NH3-free plasma enhanced chemical vapour deposition (PECVD) process detailed in [9]. Table 2 summarises the optical properties of each SiN_x layer.

The structures were defined using electron beam lithography on a high-resolution resist (ZEP520A) with a thickness of 450nm spun on the wafers. The design was then transferred to the SiN_x using inductively coupled plasma etching (ICP) with a target etch depth of 300nm and a SF_6:CHF_3 chemistry. Finally, a $1\mu m$ thick layer of PECVD SiO_x was deposited on top of the

Table 2. Optical properties of the SiN_x layers. The refractive index (n) was estimated from ellipsometry measurements. The propagation losses (PL) were measured using the cutback method as described in [9].

Wafer	Material	$\lambda = 1310nm$		$\lambda = 1550nm$	
		n	PL(dB/cm)	n	PL(dB/cm)
1	Stoichiometric	2.00	1.10	1.96	1.50
2	N-Rich	1.93	0.90	1.91	4.10
3	Si-Rich	2.57	7.50	2.54	2.30

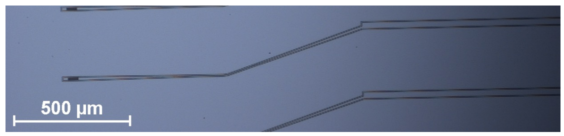

(a) Input and MDW waveguide

(b) Output and MDW waveguide

Fig. 4. Top view of the fabricated AMMI devices at the interfaces with the multimode waveguide.

devices as cladding. Figure 4 shows microscopic images of the fabricated AMMI devices.

The spectral response of the devices was characterised using two tunable laser sources with wavelength tuning ranges between 1260-1360nm (Agilent 8164B) and 1520-1620nm (Agilent 8163B). The polarisation of the light launched into the devices was controlled to ensure that only TE modes were allowed to propagate. Similarly, the chips were placed on a thermal stage to control the temperature at which the measurements were taken, so that the effect of the temperature on the spectral response of the devices could also be studied. A separate structure consisting of two tapered grating couplers connected back to back was used for normalization purposes.

3. Results and discussion

3.1. Spectral Response

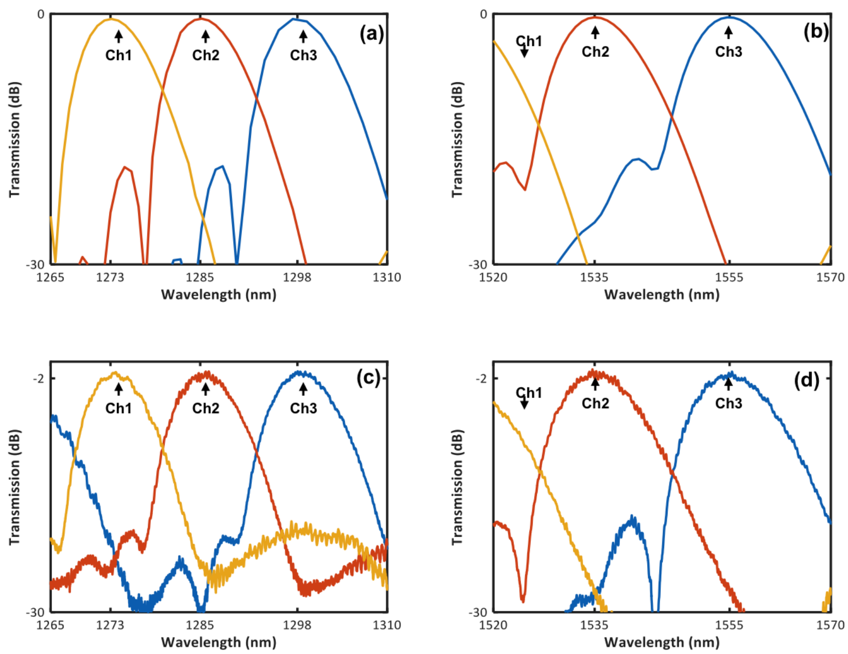

Fig. 5. Spectral response of the studied 3-channel AMMI devices on stoichiometric SiN_x ($n = 2$) at a temperature of 20°C. (a) Simulated spectra (O-band), (b) simulated spectra (C-band), (c) measured spectra (O-band) and (d) measured spectra (C-band).

Figure 5(c) and 5(d) present the transmission spectra of the two devices fabricated on the stoichiometric SiN_x (Wafer 1) measured at 20°C. The IL for both is below 2.5dB with a non-uniformity of less than 1dB across all the channels. The average 3dB bandwidth (BW) and XT for the device operating at the O-band are 7nm and <18dB respectively, while they are 10nm and <20dB for the C-band device. These experimental results are in good agreement with the theoretical simulations in 5(a) and 5(b). Moreover, the spectral response of the devices is similar to that of previously demonstrated SOI AMMIs, which have IL≈1.5-3dB, BW≈10nm and XT<15-25dB [4, 5].

3.2. *Refractive Index*

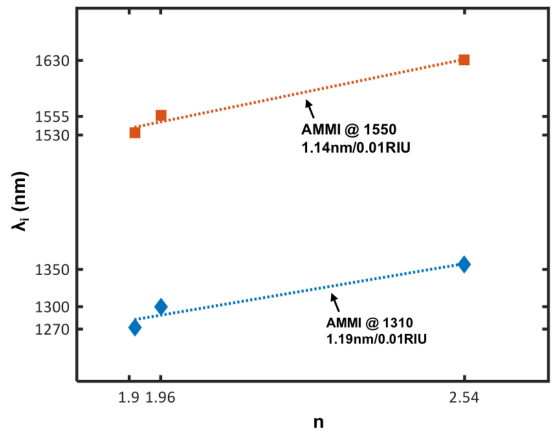

Fig. 6. Central wavelength (λ_i) as a function of the refractive index of the SiN_x layers.

Table 3. Summary of the spectral parameters of AMMIs fabricated SiN_x layers with different refractive indices.

O-band (1260-1320nm)					
Material	$\Delta\lambda$(nm)	$\Delta\lambda i$(nm)	IL(dB)	BW(nm)	XT(dB)
N-Rich	14	-25	<7.0±0.5	7	<23
Stoichiometric	13	1	<2.4±0.8	7	<18
Si-Rich	10	62	<7.6±1	6	<11
C-band (1520-1570nm)					
Material	$\Delta\lambda$(nm)	$\Delta\lambda i$(nm)	IL(dB)	BW(nm)	XT(dB)
N-Rich	19	-22	<4.2±0.5	12	<33
Stoichiometric	18	2	<2.3±0.7	10	<20
Si-Rich	15	64	<3.1±1	9	<10

Table 3 shows the spectral response of the designed AMMIs fabricated in the three different SiN_x materials. The most evident effect of changing the refractive index (n) of the SiN_x layer is the shift introduced in the central wavelength ($\Delta\lambda_i$) of the AMMI's channels. In this case, λ_i is shifted to shorter wavelengths when the n is decreased from its stoichiometric value (n = 2), while the opposite occurs when n is increased. This means that with lower n we need shorter lengths to output the desired wavelengths, while with higher n we require longer lengths. This result is important because it means that it is possible to reduce the overall footprint of the AMMI devices by using SiN_x layers with lower n. In fact, it also means that AMMIs on SiN_x can have shorter L_i than AMMIs with the same W_{MDW} on SOI because of their lower n. Figure 6 shows that the observed wavelength shift has a relatively linear behaviour that can be quantified between 1.10-1.20nm/0.01RIU at both wavelength bands.

The change in the n of the SiN_x layers not only affects $\Delta\lambda_i$, but also the overall spectral performance of the devices. The data on Table 3 show that $\Delta\lambda$ increases with decreasing n. As a result, the devices fabricated on SiN_x layers with low n tend to have a reduced channel count compared to their counterpart on SiN_x layers with high n. Nevertheless, the BW of the devices remains between 50-60% of $\Delta\lambda$'s value, which is important to ensure a lower device sensitivity to wavelength shift. Moreover, the IL non-uniformity across the channels and their XT decrease as n is reduced below its stoichiometric value (n=2) improving the performance of the devices.

In general, it can be said that the spectral characteristics improve with lower n, while they worsen with higher values. As a result, we can not only reduce the footprint of the devices using SiN_x layers with lower n, but we can improve their performance in terms of BW and XT. In fact, the XT observed in the C-band for the N-Rich AMMI is not only better than that of the stoichiometric AMMI, but is better than the typical 15-25dB XT exhibited by other WDM devices fabricated on SOI [1, 2].

Finally, it is important to note that the IL increases for the devices that were not fabricated in the stoichiometric material because their design was not optimised for the refractive index of the corresponding SiN_x. Hence, the IL can be reduced by optimising the design for the refractive index of the material layer.

3.3. AMMI Width

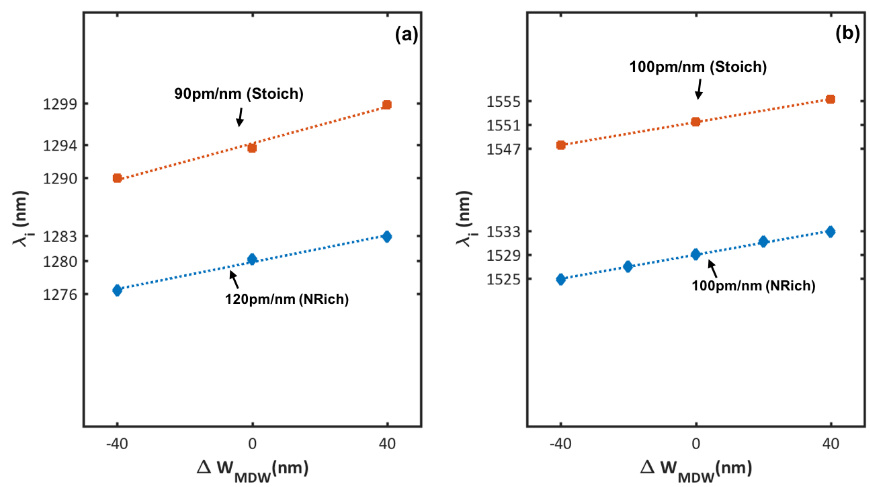

Fig. 7. Sensitivity of the spectral shift as a function of the fabrication error in the width of the AMMI's multimode waveguide observed with devices fabricated on different material layers for the (a) O-band and (b) C-band.

The sensitivity of the λ_i shift with respect to the fabrication error in the width of the AMMI's multimode waveguide was also studied (ΔW_{MDW}). Figure 7 shows the experimental results obtained in both wavelength bands for the devices fabricated on the stoichiometric and N-rich SiN_x. In this case, it can be observed that the AMMIs have almost a linear sensitivity $\Delta\lambda/\Delta W_{MDW}$ close to 100pm/nm regardless of the n of the SiN_x layer used. Table 4 shows that this value is comparable to the sensitivity of 100pm/nm observed on AMMIs previously reported on the SOI platform, [5], which in fact is already about one order of magnitude lower than that of other conventional (de)multiplexer devices [12].

These results confirm that SiN_x AMMIs have the high tolerance to dimensional errors observed in SOI AMMIs. However, SiN_x devices are known for having a considerably higher tolerance to dimensional variations due to the lower refractive index contrast between the SiN_x core and the cladding. In this case, the lack of an improved tolerance can be attributed to the width of the multimode waveguide. For single mode waveguides, the refractive index change observed with dimensional variations in SOI is ≈ 6x10^{-2}, while that observed in SiN_x is one order of magnitude smaller ≈ 7x10^{-3}. This smaller refractive index change translates into a lower sensitivity to dimensional variations in SiN_x waveguides. In the case of the MDW with $W_{MDW} = 25\mu m$, the refractive index change observed in both SOI and SiN_x is negligible. As a result, comparable $\Delta\lambda/\Delta W_{MDW}$ is expected in both platforms. The sensitivity could be potentially reduced by increasing W_{MDW} in order to decrease further the refractive index sensitivity of the multimode waveguide, but that would mean increasing the overall footprint of the devices as L_i scales with $W_{MDW}{}^2$.

Table 4. Fabrication sensitivity for different WDM devices fabricated on SOI and SiN_x. The waveguide geometry of the devices is specified by their width (W), height (H) and etch depth (ED). The sensitivity of the devices is given in both pm/nm and GHz/nm. (*This work)

Material	Device	λ (μm)	n	Waveguide (μm) W	H	ED	$\Delta\lambda/\Delta W_{MDW}$ (pm/nm)	(GHz/nm)
SOI	AWG [13]	1.55	3.5	0.5	0.22	0.22	1000	125
	RR [14]	1.55	3.5	0.5	0.22	0.13	800	99
	RR [12]	1.55	3.5	0.4	0.3	0.2	500	60
	AMMI [5]	1.55	3.5	25	0.4	0.22	100	12
SiN_x	AMMI [*]	1.31	1.93 - 2.57	25	0.3	0.3	≈100	≈17
	AMMI [*]	1.55	1.91 - 2.54	25	0.3	0.3	≈100	≈12

3.4. Temperature

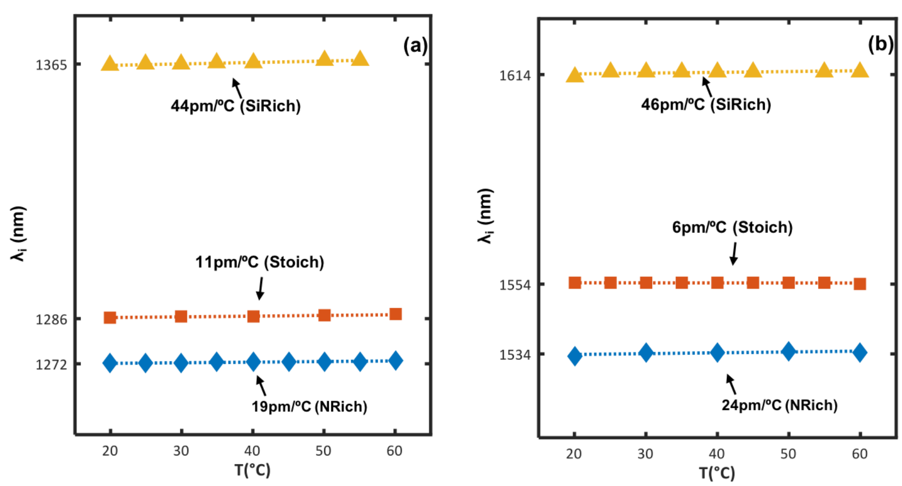

Fig. 8. Central wavelength as a function of temperature for AMMIs fabricated on different SiN_x layers operating in the (a) O-band and (b) C-band.

Figure 8 shows the central wavelength (λ_i) measured for the different AMMI devices as a function of temperature. It can be observed that in all cases λ_i increases its value as the temperature increases resulting in wavelength shifts ($\Delta\lambda/\Delta T$) between 5 and 50pm/°C that depend on the n of the SiN_x layer. The devices fabricated on the stoichiometric material have the lowest shift around 10pm/°C in both wavelength bands. On the other hand, $\Delta\lambda/\Delta T$ is higher for the devices fabricated on the N-rich layer with values close to 30pm/°C probably due to the presence of dangling bonds. Similarly, $\Delta\lambda/\Delta T$ reaches values almost as high as 50pm/°C for the devices on the Si-rich layer due to the presence of dangling bonds and the increased amount of Si atoms with a high thermo-optic coefficient within the material.

Table 5 summarizes the temperature sensitivity of different WDM devices. The $\Delta\lambda/\Delta T$ for the devices on the stoichiometric and N-rich layers is at least ≈ 8 times and 4 times better than that observed in similar (de)multiplexer devices on silicon, respectively. Moreover, it is comparable to the values observed on silica AWG devices with the advantage of having a less complex fabrication process than some compensation techniques used for Si devices.

Table 5. Temperature sensitivity for different WDM devices. Their waveguide geometry is specified by width (W) and height (H). (*This work)

Material	Device	λ (μm)	n	Waveguide (μm) W	H	$\Delta\lambda/\Delta T$ (pm/C°)
Silica	AWG [15–17]	1.55	3.5	-	-	11
Silicon	RR [3, 14, 18]	1.55	3.5	0.5	0.22	70-80
	RR [19]	1.52	3.5	0.35	0.22	54.2
	AWG [1]	1.55	3.5	0.22	0.39	72.4
SiN_x	RR [20, 21]	1.55	1.98	0.4	0.5	12-17
	AWG [22, 23]	1.31	1.98	5.5	0.05	11
	AMMI [*]	1.31	1.93	25	0.3	19
	AMMI [*]	1.31	2.00	25	0.3	11
	AMMI [*]	1.31	2.57	25	0.3	44
	AMMI [*]	1.55	1.91	25	0.3	24
	AMMI [*]	1.55	1.96	25	0.3	6
	AMMI [*]	1.55	2.54	25	0.3	44

4. Conclusions

We have demonstrated the fabrication of AMMI structures on SiN_x layers as an alternative to conventional SOI (de)multiplexers. We have shown that stoichiometric SiN_x layers can be used to fabricate AMMIs with XT<20dB and IL<3dB. This performance is comparable to the state of art of AMMIs on the SOI platform with the advantage of having a $\Delta\lambda$ below 10pm/°C, which is at least 8 times lower than the one observed in typical SOI (de)multiplexers. We have also demonstrated that devices fabricated on N-rich layers have the potential to achieve XT values even below 30dB with a $\Delta\lambda$/°C of 20pm/°C. These XT values are lower than the typical 15-25dB observed in other WDM devices fabricated on SOI.

In addition, we have demonstrated that the AMMI devices fabricated in SiN_x require smaller L_i thus reducing their overall footprint, whereas the footprint of other SiN_x structures, such as AWGs and PCGs, increases by almost an order of magnitude due to their lower refractive index contrast compared to SOI. Nevertheless, the size of the multimode waveguide limits the tolerance to fabrication errors of the devices to values close to 100pm/nm which are comparable to those of other AMMIs in SOI. The sensitivity to dimensional variations could be reduce by increasing W_{MDW} at a price of increased device footprint.

As a result, we have proved that SiN_x AMMIs are a convenient option to fabricate athermal (de)multiplexers with a good tolerance to fabrication errors and temperature variations with a relatively simple fabrication process. The studied devices have the potential to be used for commercial applications that are sensitive to temperature variations, but there is still room for improvement. In fact, both the size and the performance of the AMMIs could be improved by optimizing the design for SiN_x layers with a refractive index close to a N-rich composition because L_i decreases and the spectral performance of the devices improves with lower n.

Funding

H2020 European Research Council (688516); Engineering and Physical Sciences Research Council (EPSRC) (EP/L021129/1, EP/N013247/1).

Aknowledgments

The authors acknowledge the financial support from the above listed funding bodies. Domínguez Bucio would like to thank the Optoelectronics Research Centre (ORC) and CONACyT for their support to pursue doctoral studies. The fabrication was carried out at the Southampton Nanofabrication Centre, University of Southampton, UK. All data supporting this study are openly available from the University of Southampton repository at http://doi.org/10.5258/SOTON/D0178.